Multi-body Dynamics Study of Gears

Behara Neha

Computer Aided Conception and Production in Mechanical Engineering

September 9, 2022

in Vertretung für Institutsdirektor Prof. Dr.-Ing. Stefan Reh
Institut für Test und Simulation für Gasturbinen, DLR:

i. V.

C=DE, O=Deutsches Zentrum fuer Luft- und Raumfahrt e.V. (DLR), CN=Olga Riemer
Augsburg

Contents

1 Introduction

One of the key factors in the determination of gear reliability, and by extension, transmission life, is the dynamic loading on the gear teeth. The most important criterion in the estimation of gear reliability is ensuring safety throughout its lifetime. This reliability becomes more crucial in helicopters and aircraft transmissions because the safety risk is high and transmission failure could be catastrophic. Gears have also been employed in aeroengines to improve the engine efficiency by increasing the propulsion efficiency. A planetary gear system reduces the shaft's speed from the turbine to the fan, which allows the low-pressure (LP) shaft to run at higher rotational speed [1]. The lower fan speed offers higher bypass ratios, resulting in better fuel consumption and noise reduction (Figure 1). Also, double helical gears are usually preferred over spur gears because the former offers significantly higher load carrying capacity without the problem of axial thrust as in helical gears. [2]

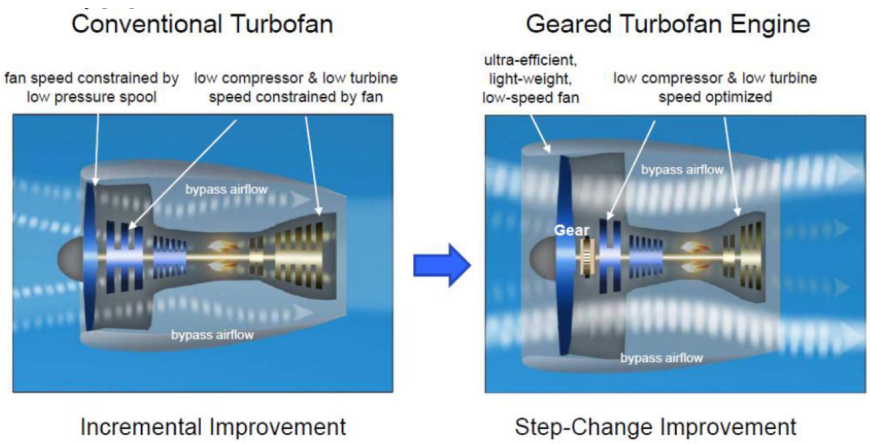

Figure 1: Comparison between conventional turbofan and geared turbofan architecture [1]

To understand gear design, it is important to study the dynamic response caused by gear meshing and the vibrations resulting from it. Due to cyclic and irregular loading, these vibrations may lead to tooth pitting and cracking [3]. Tooth fracture is one of the main failure forms in gears. Under normal circulatory loading conditions, fatigue cracks occur at tooth root and propagate gradually [4]. Hence, the load carrying capacity is to be studied for minimizing tooth wear. The objective of this current work is to determine the crack propagation in a gear subject to dynamic loading and investigating

vibrations to characterize influence of the crack. Therefore, mathematical models are needed to evaluate the dynamic behavior of the system under loading and propagating crack.

This study is a summary of methodology progress being followed to estimate the crack propagation path in a three-gear system- a planetary gear between two sun gears (Figure 2). A simplification of problem steps is done to understand the body dynamics as per the loading conditions. An overview of the significance of crack propagation studies and the state-of-the-art simulation techniques is required for this simplification. The effectiveness of these methods, the advantages and shortcomings are summarized. The study then moves its course to the process of designing a healthy gear as a prerequisite to crack propagation study. A simpler system of gears is taken into consideration first to study the loading and vibration characteristics. Finally, to understand how a multi degree of freedom system works, a numerical model of spring mass damper with two degrees of freedom is set up.

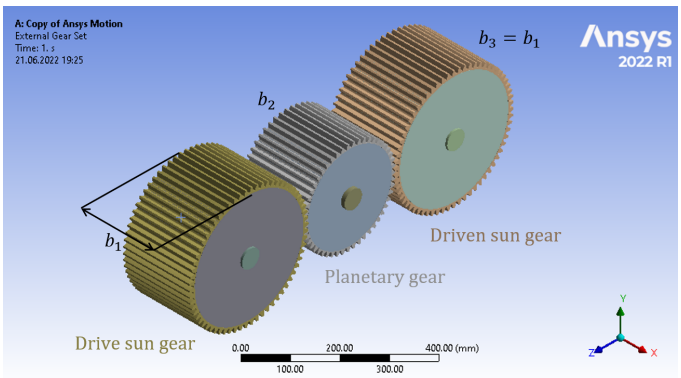

Figure 2: Reference gear setup

2 Motivation

Gear faults can usually occur due to fatigue, spalling or pitting caused by wear, load fluctuations, backlash etc. [5]. This severely reduces actual strength of the gears and prompts crack growth. Fatigue cracks may appear in the region of highest stresses, whose location can be determined based on numerical analysis, meshing force variability, point of application and its direction [6]. So, an understanding of the tooth failure mechanism is needed to design more reliable gears. Numerical methods are one of the techniques to study crack initiation and propagation and are discussed here.

3 State of the Art

A study by Jelaska and Glodez [7] uses a computational model with respect to bending fatigue in a gear tooth root, where the fatigue process is divided into crack initiation and propagation period. The fatigue crack initiation threshold is determined, with the assumption being that the initial crack is located at the point of largest stresses in the tooth root. The study uses Linear Elastic Fracture Mechanics to describe the crack growth rate. The crack length for crack propagation from the initiation to the critical crack length is numerically estimated using the Finite Element Method with FRANC2D. The FE mesh around the initial crack in a gear tooth root is shown in Figure 3. In the numerical computations, it has been assumed that Linear Elastic Fracture Mechanics, a tool for life expectancy estimation of cracked components [8], is not valid below some threshold crack length. The crack extension angle is the predicted according to the Maximum Tensile Stress criterion.

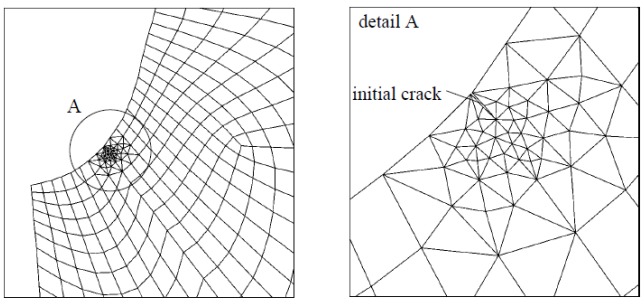

Figure 3: Finite element mesh around initial crack in a gear tooth [7]

A number of studies have focused on the effect of crack on bending mesh stiffness. Chaari and Fakhfakh [9] analyze the effect of a tooth crack on the bending stiffness, with shape of the crack approximated as a straight line to simplify the problem. It is observed that gear mesh stiffness decreases and maximum effect of tooth crack is observed when load is applied at addendum circle of the defective tooth.

A study by Chen and Shao [10] describes an analytical model to investigate the effect of gear tooth crack on mesh stiffness, considering crack propagation both along and through tooth width. Tooth deflections are calculated by potential energy method based on beam theory. Besides tooth deflection, it has been found that fillet-foundation deflection also influences stiffness. The mesh stiffness plots with varying crack lengths are illustrated below. It

is apparent from Figure 4 that maximum stiffness reduction is encountered when the cracked tooth of pinion is just going to engage.

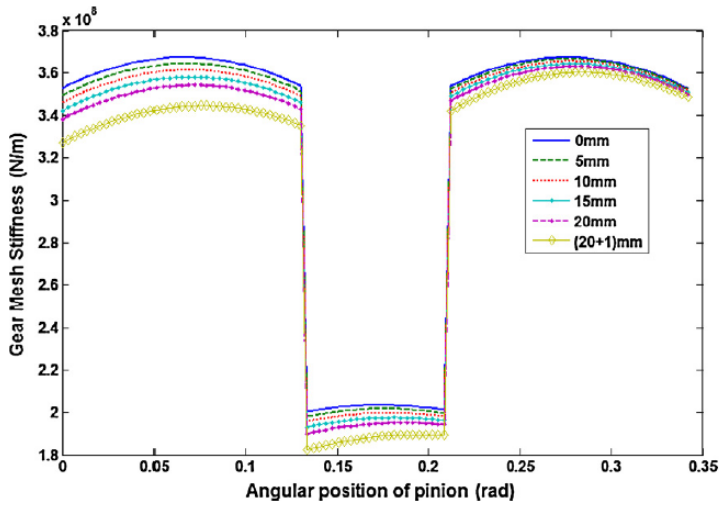

Figure 4: Mesh stiffness with different crack length along tooth width [10]

A study by Shao [4] uses cracked beam theory to analyze the gear dynamic characteristics. It considers the tooth as a cantilever beam (Figure 5) and devises a three-dimensional finite element numerical analytical model. The dynamics natural characteristics of gear structure with crack are investigated, e.g., natural frequency, vibration shape, dynamic stress and the effects with different lengths and positions are simulated. A theoretical foundation is

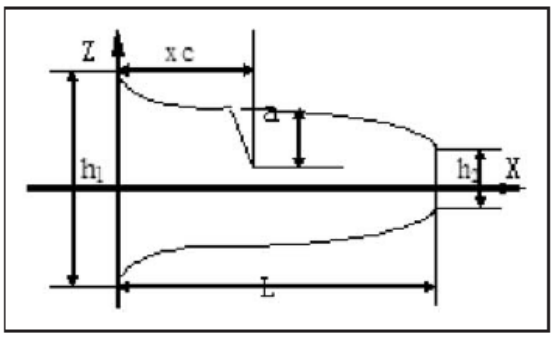

Figure 5: Model of cracked gear tooth [4]

established for identifying gear crack and lay a good foundation for further crack detection through acoustic characteristics analysis. A mathematical

model for cracked gear is set up based on the Hu-Washizu variation integral principle with boundary conditions set on the principle that the strain energy density increases for a beam dynamic system.

A study by Endeshaw and Osire [3] discusses a foundation with a dynamic model of a one-stage gearbox, a finite element method, and a degradation model for the estimation of fatigue crack propagation in gear. The six degrees of freedom gearbox is modeled on MATLAB. Potential energy method used to perform the mesh stiffness calculation. In this method, total potential energy stored in mesh gear system includes four components: Hertzian energy, bending energy, shear energy and axial compressive energy, which can be used to calculate the corresponding mesh stiffness [11]. The force calculation considers the maximum torque values used in the dynamic modeling.

As, the paper focuses on estimation of crack propagation, meshing around the crack tip (Figure 6) is emphasized to obtain accurate nodal displacements near crack tip from displacement correlation method. Model generation and solving for nodal displacements has been done on ANSYS, with the assumption being that the accuracy of the nodal displacements is not affected by the non-homogeneity of the mesh. The framework followed is summarized in the flowchart in Figure 7.

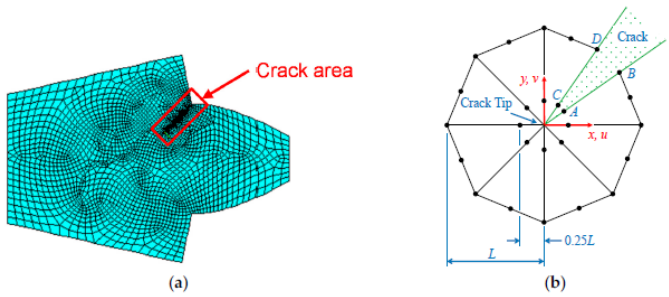

Figure 6: Finite element model for: (a) cracked gear tooth; and (b) singular element at the crack tip [3]

A recent work by Chen and Huangfu [12] considers the complex foundation structure with the real spatial crack propagation path under partial load simulated by Extended Finite Element Method (XFEM). For the XFEM, the crack is constructed by cohesive segment method which includes mainly three

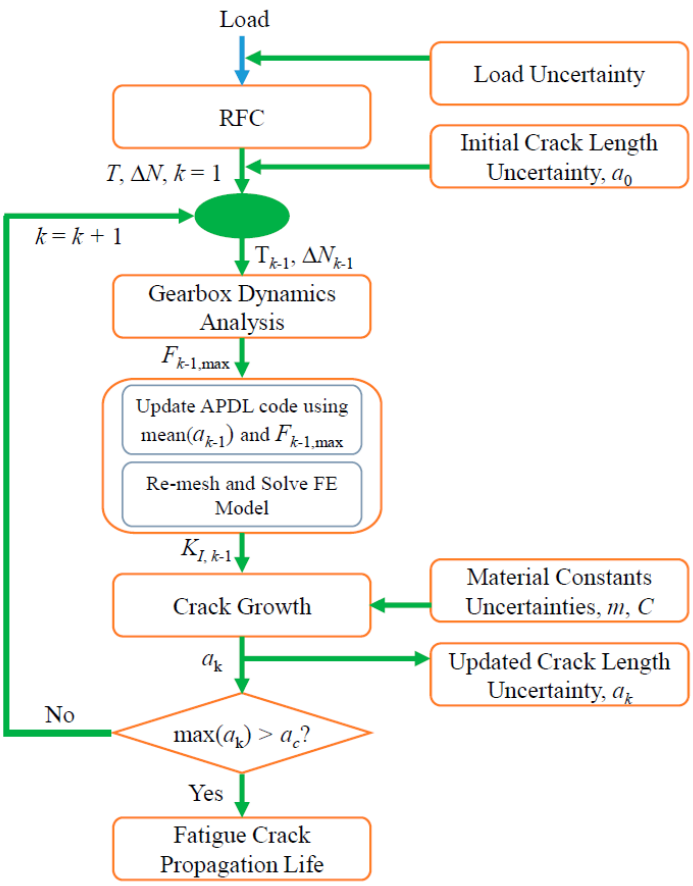

Figure 7: Framework for fatigue crack propagation in APDL- ANSYS Parametric Design Language [3]

factors- the initial damage criterion, the direction criterion and damage evolution criterion. First, the maximum principal stress at crack location is derived from the Finite Element Model. When initial identification parameter of damage satisfies the limit discriminant coefficient relation, a new cohesive segment is inserted in the next propagation step.

4 Problem Formulation

Before delving into crack propagation, it is essential to design a healthy gear pair model. A planetary helical gear system is quite complex to begin with. To understand the dynamic response, a number of studies have focused on simplification to a spur gear system, which are discussed in the next

section.

5 Study and Analysis

In a study by Rezaei and Poursina [13], analytical equations are derived for spur gear pair. As helical gears are taken into consideration, a helical tooth is divided into several independent thin spur tooth slices and mesh stiffness is calculated (Figure 8). The slices are considered with no connections between them, making this study limited to gears with low helix angles. The spur gear is considered as a beam according to the potential energy method and the axial, bending and shear and fillet-foundation stiffness for each gear is calculated. The analytical results are then compared with the Finite Element Method in ABAQUS software.

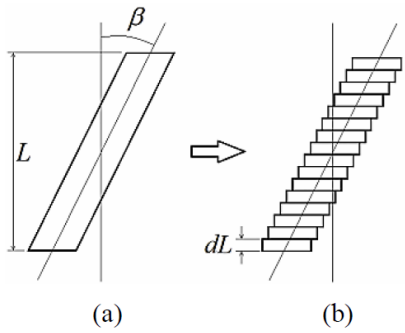

Figure 8: (a) Helical tooth; (b) sliced thin spur teeth [13]

Lumped parameter models have widely been used in gear pair modeling. These usually involve the assumption of shafts and bearings to be rigid and representation of gear mesh with a parallel combination of spring and damper system. The models can be extended to include static or dynamic transmission error, backlash and a time-varying mesh stiffness. The numerical simulations can then be solved using Runge-Kutta method or other integration methods. Also, the vibration levels significantly change between a constant load conditions and time-varying load conditions and constant damping and time-varying damping conditions.

A robust analytical framework has been well illustrated by Robert Parker [14] for modeling and understanding planetary gear dynamics and examine some factors affecting gear vibration. A lumped parameter model has been

derived for spur planetary gears including mesh stiffness variation and transmission error excitation, which has been considered valid for general epicyclic gears with any number of planets. So, this is a generalized study that can be used as a fundamental tool for specialized cases. The natural frequency spectra and vibration modes have been analyzed, with cases including diametrically opposed planets. Eigensensitivities are obtained from vibration mode properties. Finally, the parametric instabilities caused by time-varying mesh stiffness are investigated. The modal properties are used to identify the effects of contact ratios and mesh phasing on parametric instabilities. This study has been performed on a spur gear model for two-dimensional analysis, as helical gears require a three-dimensional analysis.

A multi-mesh system will make the oscillations become more complex. Such a system has been studied by Jiang and Shao [15], where to illustrate complex oscillation phenomena, an eight degree of freedom non-linear dynamic model of a multi-mesh gear (Figure 9) is developed to study the responses of the system. Interactions between these mesh stiffness variations at the two meshes are analyzed.

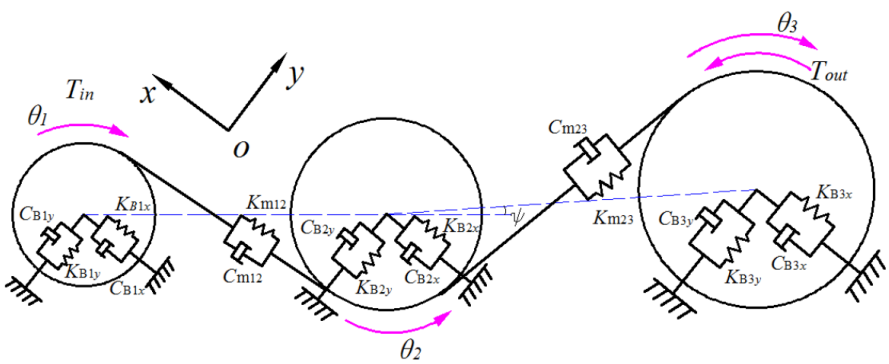

Figure 9: Dynamic model of the multi-mesh gear system [15]

This work is particularly interesting to the cause of the current study as it also involves a gear between two diametrically opposite sun gears. The mesh combinations are simulated as spring-damper pairs and the effect of friction is neglected here with the added assumption that the mean load is high and the dynamic load is insufficient to cause tooth separations (no contact loss). The mess stiffness variation occurs due to the alternating engagement of single tooth pairs and double tooth pairs. This study also uses the Runge-Kutta 4th and 5th order algorithm with a fixed time step to numerically integrate the governing equations.

It is advantageous to have a comparison between analytical and Finite Element Method for analysis of gear dynamics. A study by Ambarisha and Parker [16] has shed some light on this comparison. The work examines the nonlinear dynamic behavior of spur planetary gears using two models of lumped-parameter model and a finite element model. The two-dimensional model represents the gears as lumped inertias, the gear meshes as nonlinear springs with tooth contact loss and periodically varying stiffness due to changing tooth contact conditions, and the supports as linear springs (Figure 10). The governing equation can be given by:

$$M\ddot{x} + C\dot{x} + K(x,t)x = F(t) \tag{1}$$

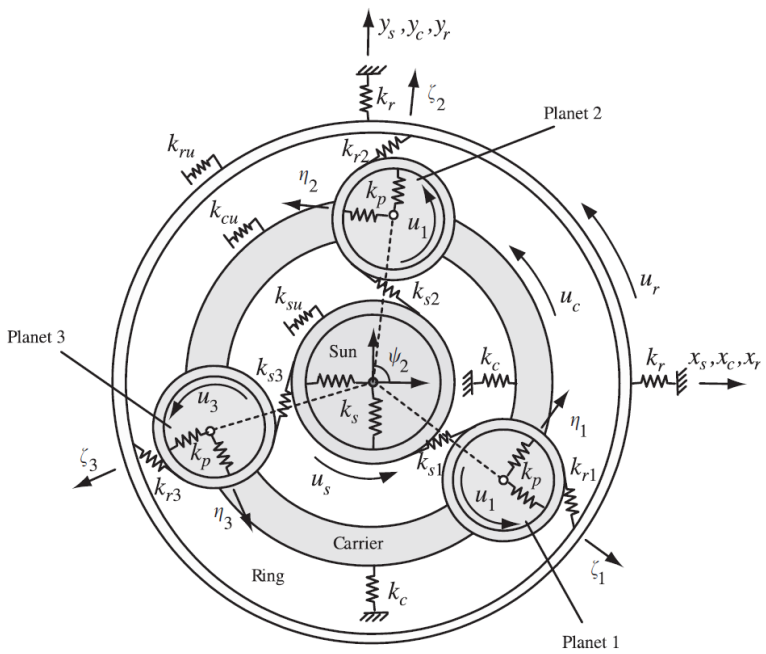

Figure 10: Planetary gear lumped-parameter analytical model [16]

Mesh stiffness variation excitation, corner contact, and gear tooth contact loss are all intrinsically considered in the FE analysis. Finite element-contact analysis software Calyx, which is specialized for gear dynamics is used to model the planetary gears. The software uses combined surface integral and finite element solution, which reduces the number of finite elements and facilitates analysis with reasonable run times. Mesh stiffness variation due

to change in number of teeth in contact, contact due to elastic deformation of gear teeth, contact loss are intrinsically modeling in FE model. The only additional inputs to gear geometry and material properties are input torque and the gear speed. As transmission error is also a computed output, there is no need to assume a static transmission error. A huge advantage of this model is that it reduces the number of assumptions.

The final steady-state response at a particular speed is used as the initial condition for the next speed. The equation (1) is solved using a fourth order Runge-Kutta integration method. Responses from the dynamic analysis using analytical and FE models are successfully compared qualitatively and quantitatively. These comparisons validate the effectiveness of the lumped-parameter model to simulate the dynamics of planetary gears. A similar approach will be helpful to validate the analytical model for simpler models considered in this case, which will be focused on at a later stage of the study.

5.1 Spur-gear pair with time-variant loading

A research by Yousfi [17] identifies damping model in the gear system with time-varying stiffness and time-varying excitation forces. The model consists of a spur gear pair with time-variant loading (Figure 11). The two differential equations of gear system can be given by Newton's laws of motion.

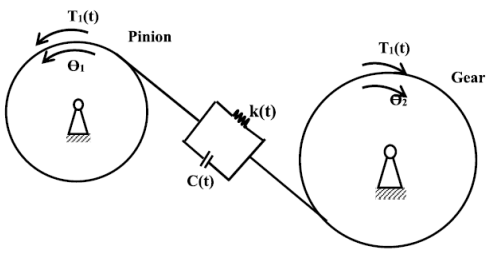

Figure 11: Dynamic model of a spur-gear pair system[17]

$$\mathrm{I}_1\frac{\mathrm{d}^2\theta_1}{\mathrm{dt}^2} + \mathrm{R}_1\mathrm{c(t)}(\mathrm{R}_1\frac{\mathrm{d}\theta_1}{\mathrm{dt}} - \mathrm{R}_2\frac{\mathrm{d}\theta_2}{\mathrm{dt}}) + \mathrm{R}_1\mathrm{k(t)}(\mathrm{R}_1\theta_1 - \mathrm{R}_2\theta_2)) = \mathrm{T}_1\mathrm{(t)} \quad (2)$$

$$\mathrm{I}_2\frac{\mathrm{d}^2\theta_2}{\mathrm{dt}^2} - \mathrm{R}_2\mathrm{c(t)}(\mathrm{R}_1\frac{\mathrm{d}\theta_1}{\mathrm{dt}} - \mathrm{R}_2\frac{\mathrm{d}\theta_2}{\mathrm{dt}}) - \mathrm{R}_2\mathrm{k(t)}(\mathrm{R}_1\theta_1 - \mathrm{R}_2\theta_2)) = -\mathrm{T}_1\mathrm{(t)} \quad (3)$$

where R_1 and R_2 are the radii of the two gears, m_1 and m_2 are the two masses, I_1 and I_2 are the moments of inertia, θ_1 and θ_2 are the two rotation degrees of freedom.

The mesh-stiffness variation is presented using the square waveform as follows:

$$k(t) = \begin{cases} K_{max} \; .... \; for \; 0 < t < (\varepsilon_\alpha - 1)T_e \\ K_{min} \; .... \; for \; (\varepsilon_\alpha - 1)T_e < t < T_e \end{cases} \tag{4}$$

where T_e is the meshing period, ϵ_α is the contact ratio and K_{max} and K_{min} are the extreme values of stiffness. Rewrite equation (2) and (3) with M_e as equivalent mass and dynamic transmission error as y

$$y = R_1\theta_1 - R_2\theta_2 \tag{5}$$

$$M_e\frac{\mathrm{d}^2y}{\mathrm{d}t^2} + c(t)\frac{\mathrm{d}y}{\mathrm{d}t} + k(t)y = M_e(\frac{R_1}{I_1} + \frac{R_2}{I_2})T_1(t) \tag{6}$$

$$M_e = \frac{I_1 I_2}{I_1 R_2^2 + I_2 R_1^2} \tag{7}$$

In non-dimensional form, the equation can be written as:

$$\frac{\mathrm{d}^2y}{\mathrm{d}t^2} + C(t)\frac{\mathrm{d}y}{\mathrm{d}t} + K(t)y = F(t) \tag{8}$$

$$F(t) = \frac{T_1(t)R_1}{I_1} + \frac{T_1(t)R_2}{I_2} \tag{9}$$

where F(t) is the time-varying external excitation, K(t) is the time-varying rigidity and C(t) is the unknown damping. A constant piecewise model (Figure 12) is presented for damping, where the damping is considered constant in each defined time interval.

$$C(t) = \begin{cases} C_0 \; .... \; for \; T_0 < t < T_1 \\ C_1 \; .... \; for \; T_1 < t < T_2 \\ . \\ . \\ C_{n-1} \; .... \; for \; T_{n-1} < t < T_n \end{cases} \tag{10}$$

The damping values are then solved by the integral method, where Eq. 8 is integrated with respect to time. The unknown parameters of the integral

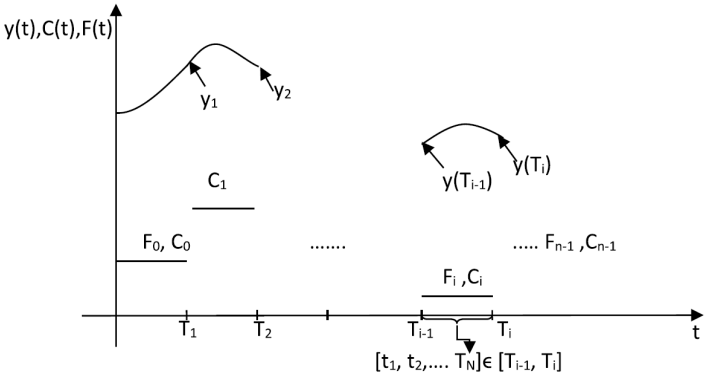

Figure 12: Piecewise Model of the observed response and damping C(t) [17]

method are obtained using the linear least squares method in matrix form. The idea is to transform the observed data by the integral operator, which is created by MATLAB. The evaluation of time-varying stiffness presented in the paper (Figure 13) or damping evaluation is outside the scope of this internship. In this study, the performance of the proposed method of damping calculation is validated based on a simulated example. The free response is simulated using second order Runge-Kutta procedure.

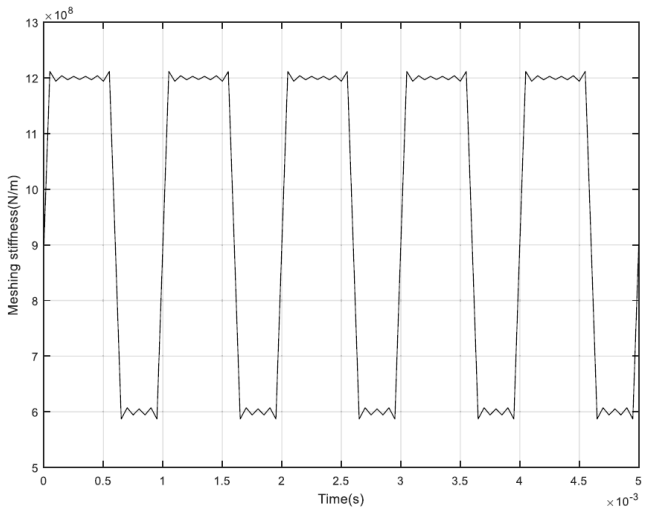

Figure 13: Time-varying mesh stiffness [17]

5.2 Spring Mass Damper System

A similar methodology is used in this study to observe the dynamic behavior of a spring mass damper system. The system is considered to replicate the gear mesh, which is often represented by a parallel connection of a spring damper system. Figure 14 shows a 2DOF Mass spring damper system. The system is subjected to an external force on mass m_1 in the outward direction.

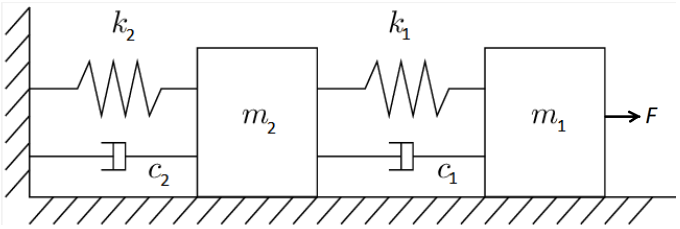

Figure 14: Two mass spring damper system

The parameters of the system have been summarized in Table 1. The

Table 1: Spring damper system parameters

Parameter	**Symbol**	**Block 1**	**Block 2**	**Unit**
Mass	m	3	15	kg
Spring Constant	k	10	100	N/m
Damping Ratio	ζ	0.02	0.1	Ns/m
Initial Displacement	x	0	0	m

equations of motion for the two masses can be given by:

$$m_1\ddot{x_1} + \dot{x_1}(c_1 + c_2) - c_2\dot{x_2} + x_1(k_1 + k_2) - k_2x_2 = F \tag{11}$$

$$m_2\ddot{x_2} + c_2\dot{x_2} - c_2\dot{x_1} + k_2x_2 - k_2x_1 = 0 \tag{12}$$

Substituting second order terms to get a system of first-order Ordinary Differential Equations
$u_1 = x_1$ and $u_2 = \dot{x_1}$
$w_1 = x_2$ and $w_2 = \dot{x_2}$

Rewriting the equations of motion,

$$\dot{u_2} = \frac{1}{m_1}(-(c_1 + c_2)u_2 - c_2w_2 + (k_1 + k_2)u_1 - k_2w_1 + F) \tag{13}$$

$$\dot{w_2} = \frac{1}{m_2}(-c_2w_2 + c_2u_2 - k_2w_1 + k_2u_1) \tag{14}$$

In addition to the Euler method, State space representation method is tested. The state space is a control method that can reflect the changes of internal dynamic characteristics and the relationship between the input state and externa factors. It is a suitable method for solving complex dynamic problems of multi-degree of freedom systems with multiple inputs and multiple output variables, nonlinear systems and time-varying systems [18]. The state space representation can be given as:

$$\begin{bmatrix} \dot{u}_1 \\ \dot{u}_2 \\ \dot{w}_1 \\ \dot{w}_2 \end{bmatrix} = \begin{bmatrix} 0 & 1 & 0 & 0 \\ \frac{-k_1}{m_1} & \frac{-c_1}{m_1} & \frac{k_1}{m_1} & \frac{c_1}{m_1} \\ 0 & 0 & 0 & 1 \\ \frac{k_1}{m_2} & \frac{c_1}{m_2} & \frac{-(k_1+k_2)}{m_2} & \frac{-(c_1+c_2)}{m_2} \end{bmatrix} \begin{bmatrix} u_1 \\ u_2 \\ w_1 \\ w_2 \end{bmatrix} + \begin{bmatrix} 0 \\ \frac{1}{m_1} \\ 0 \\ 0 \end{bmatrix} F \tag{15}$$

The simulations are performed on Python to get the displacement, velocity and acceleration responses against time (Figure 15).

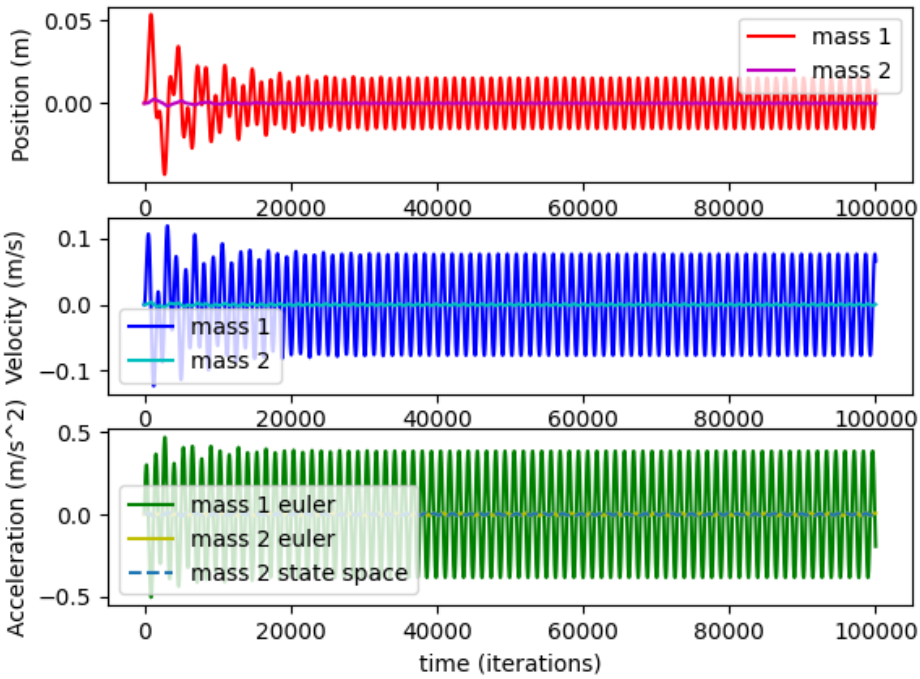

Figure 15: Positions, velocities and accelerations of the masses

We can see the decaying response and the stability region for the two masses. There is also an option to observe the step response of the system

in absence of the external force and providing only initial displacements to the two blocks. In addition, the state space representation and Euler method do not provide different results here(Figure 16). However, Euler method will not work for more complicated systems, as the method is only first order convergent and very small time steps (0.001s here)are required to achieve satisfactory results [19]. As a number of models have performed the equation solving methodology with Runge-Kutta 4th order, it will be advantageous to compare the Euler and state space representation with Runge-Kutta method (as a part of future study).

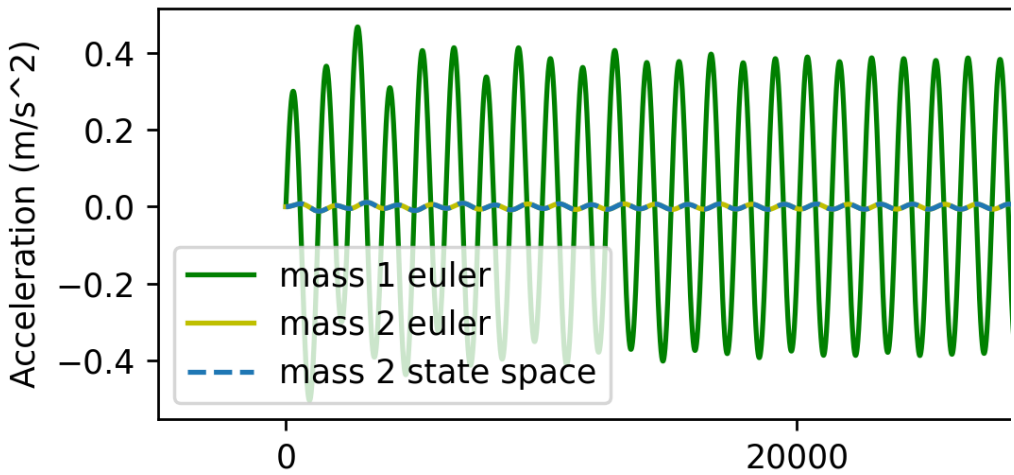

Figure 16: Comparison of State space and Euler method

The hanning cut signal (Figure 17) is being used here for leakage protection with good amplitude accuracy. The advantage of Hanning Window is that it reduces the side lobes. It has good frequency resolution and is better for identifying smaller-magnitude components from the larger ones [20]. The filter coefficients of a Hanning window is characterized by the formula [21]:

$$w(n) = 0.5(1 - cos(2\pi\frac{n}{N})), 0 \leq n \leq N \tag{16}$$

where length of window is $N + 1$.

We can see from Figure 17 that the Hanning window is able to suppress discontinuity in the frequency analysis by tapering the signal soothly towards zero at the start and end of the recording window, which is necessary for receiving a reasonable FFT analysis. If a window function is not used, a non-zero start and end value can deliver incorrect results in investigating

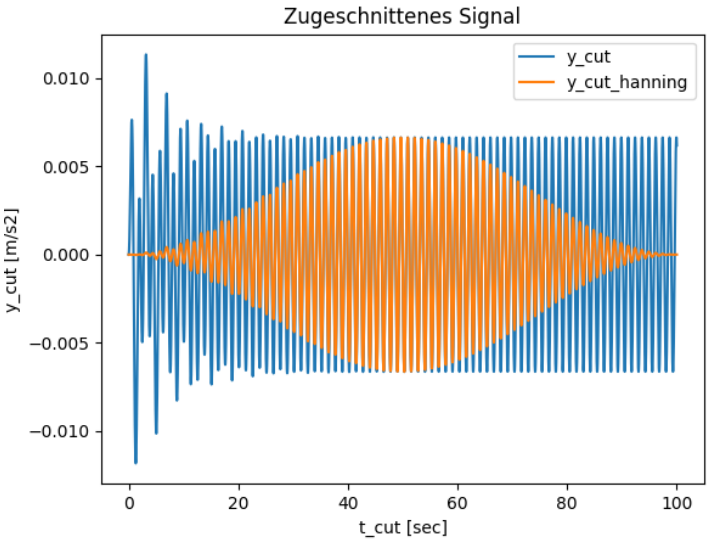

Figure 17: Hanning cut signal

a continuous time signal. The zeros and poles of the dynamic system are plotted to get eigenvalues, and establish stability criteria (Figure 18). As the system differential equation represents the transfer function, its roots define the system poles and effectively the system response. So, the transfer function poles are the roots of the equation and also the eigenvalues of the state space system matrix [22].

A few inferences can be drawn from the location of poles from the plot in Figure 19. First, the eigenvalues of the system in Eq. 15 are calculated, given as follows:

[-6.02720084+0.j
-0.14261096+1.8026355j
-0.14261096-1.8026355j
-1.12757724+0.j]

The real poles on the left-half of the plane signify an exponentially decaying component in the response. The other two poles are complex conjugate pair generate a response component of a decaying sinusoid, where amplitude and frequency is determined by initial conditions. The zero-pole plot is particularly informative in establishing the relation between pole locations, natural frequency and damping ratio. The natural frequency is the length

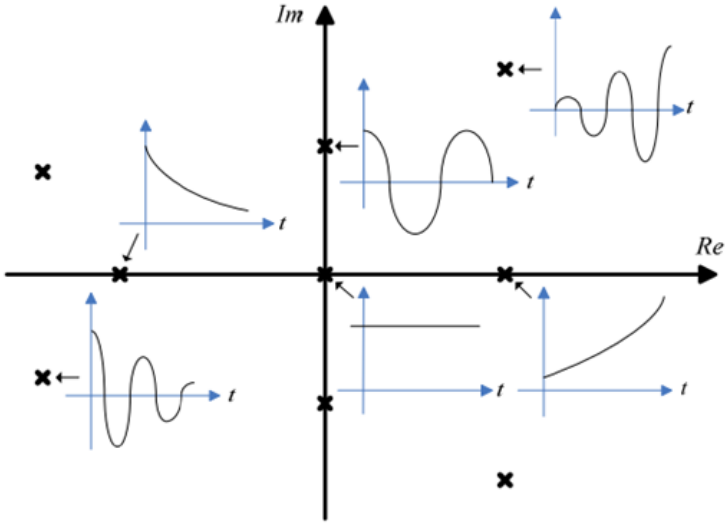

Figure 18: Influence of pole position on system response [23]

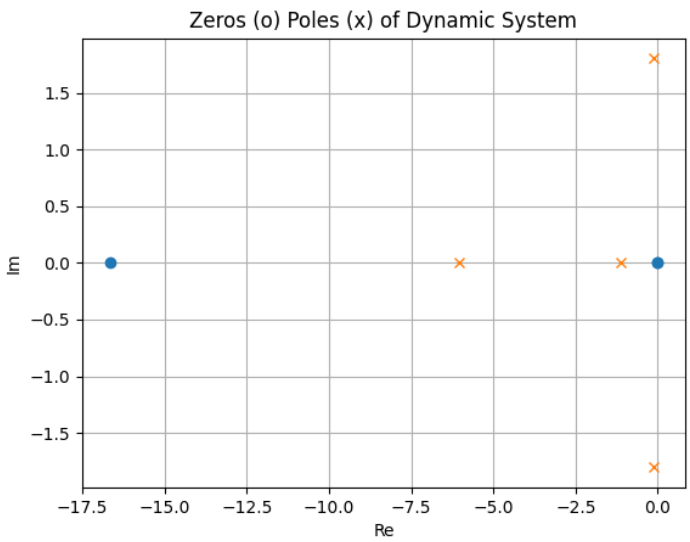

Figure 19: Zeros and poles of the system

of the vector from the origin to either of the complex poles. The imaginary part of the pole is the "damped natural frequency"; this is the frequency of oscillation when the poles are excited. The real part of the poles sets the rate at which the oscillation envelope decays [24].

6 Conclusion

This study is a summary of some of the work done in modeling gear dynamics, including some simplifications done to study the segments of the desired system better. A numerical model for studying multi-degree of freedom system is established. There is a need to experiment with different methodologies (time-integration methods like Euler, Euler-Cromer, Runge-Kutta, state space etc.) to compare them for the ease and accuracy of modeling strategies. Analytical models have been the focus of this study because the computational cost with using only Finite Element models is very high. In future study, a semi-analytic method coupled with FEM will furnish better results.

7 References

[1] A. M. Tobi and A. Ismail, "Development in geared turbofan aeroengine," in *IOP Conference Series: Materials Science and Engineering*, vol. 131, p. 012019, IOP Publishing, 2016.

[2] K. Kawasaki, I. Tsuji, and H. Gunbara, "Manufacturing method of double helical gears using multi-axis control and multitasking machine tool," in *International Gear Conference*, pp. 86–95, 2014.

[3] H. B. Endeshaw, S. Ekwaro-Osire, F. M. Alemayehu, and J. P. Dias, "Evaluation of fatigue crack propagation of gears considering uncertainties in loading and material properties," *Sustainability*, vol. 9, no. 12, p. 2200, 2017.

[4] R. Shao, P. Jia, and F. Dong, "Dynamic characteristics of cracked gear and three-dimensional crack propagation analysis," *Proceedings of the Institution of Mechanical Engineers, Part C: Journal of Mechanical Engineering Science*, vol. 227, no. 6, pp. 1341–1361, 2013.

[5] P. Sopcik and D. O'Sullivan, "How sensor performance enables condition-based monitoring solutions," *5 Making Sense of Sounds, or How AI Can Boost Your Machines' Uptime*, p. 45, 2019.

[6] J. Maczak and M. Jasinski, "Model-based detection of local defects in gears," *Archive of Applied Mechanics*, vol. 88, no. 1, pp. 215–231, 2018.

[7] D. T. Jelaska, S. Glodez, and S. Podrug, "Numerical modelling of the crack propagation path at gear tooth root," in *International Design Engineering Technical Conferences and Computers and Information in Engineering Conference*, vol. 37025, pp. 201–207, 2003.

[8] H. D. Bui, J. Leblond, and N. Stalin-Muller, "Background on fracture mechanics," 2001.

[9] F. Chaari, T. Fakhfakh, and M. Haddar, "Analytical investigation on the effect of gear teeth faults on the dynamic response of a planetary gear set," *Noise Vibration Worldwide*, vol. 37, no. 8, pp. 9–17, 2006.

[10] Z. Chen and Y. Shao, "Dynamic simulation of spur gear with tooth root crack propagating along tooth width and crack depth," *Engineering failure analysis*, vol. 18, no. 8, pp. 2149–2164, 2011.

[11] Z. Wan, H. Cao, Y. Zi, W. He, and Y. Chen, "Mesh stiffness calculation using an accumulated integral potential energy method and dynamic analysis of helical gears," *Mechanism and Machine Theory*, vol. 92, pp. 447–463, 2015.

[12] K. Chen, Y. Huangfu, Z. Zhao, H. Ma, and X. Dong, "Dynamic modeling of the gear-rotor systems with spatial propagation crack and complicated foundation structure," *Mechanism and Machine Theory*, vol. 172, p. 104827, 2022.

[13] M. Rezaei, M. Poursina, S. H. Jazi, and F. H. Aboutalebi, "Calculation of time dependent mesh stiffness of helical planetary gear system using analytical approach," *Journal of Mechanical Science and Technology*, vol. 32, no. 8, pp. 3537–3545, 2018.

[14] R. G. Parker, J. Lin, and T. L. Krantz, "Modeling, modal properties, and mesh stiffness variation instabilities of planetary gears," tech. rep., 2001.

[15] H. Jiang and Y. Shao, "Dynamic analysis of a multi-mesh gear system with mesh stiffness variation," in *International Design Engineering Technical Conferences and Computers and Information in Engineering Conference*, vol. 55928, p. V005T11A014, American Society of Mechanical Engineers, 2013.

[16] V. K. Ambarisha and R. G. Parker, "Nonlinear dynamics of planetary gears using analytical and finite element models," *Journal of sound and vibration*, vol. 302, no. 3, pp. 577–595, 2007.

[17] N. Yousfi, B. Zghal, A. Akrout, L. Walha, and M. Haddar, "Estimation of the damping model of a spur gear pair system including a time-varying loading," *Comptes Rendus. Mecanique*, vol. 350, no. G2, pp. 255–267, 2022.

[18] Z. Cao, Y. Chen, G. Li, L. Zang, D. Wang, Z. Qiu, and G. Wei, "Dynamic simulation and experimental study of electric vehicle motor-gear system based on state space method," *Machines*, vol. 10, no. 7, p. 589, 2022.

[19] S. Linge and H. P. Langtangen, *Programming for Computations-Python: A Gentle Introduction to Numerical Simulations with Python 3.6*. Springer Nature, 2020.

[20] D.-J. Jwo, I.-H. Wu, and Y. Chang, "Windowing design and performance assessment for mitigation of spectrum leakage," in *E3S Web of Conferences*, vol. 94, p. 03001, EDP Sciences, 2019.

[21] V. Giurgiutiu, *Structural health monitoring: with piezoelectric wafer active sensors*. Elsevier, 2007.

[22] J. Rommes and N. Martins, "Computing transfer function dominant poles of large-scale second-order dynamical systems," *SIAM Journal on Scientific Computing*, vol. 30, no. 4, pp. 2137–2157, 2008.

[23] B. Lohmann, "Skriptum regelungstechnik," 2017.

[24] M. T. Thompson, "Review of signal processing basics," *Intuitive Analog Circuit Design*, pp. 15–52, 2014.